

1 **TITLE Post processing the U.S. National Water**
2 **Model with a Long Short-Term Memory network**

3 **Jonathan M. Frame ¹, Grey S. Nearing^{1,2}, Frederik Kratzert³, Austin Raney ⁴**
4 **& Mashrekur Rahman ¹**

5 ¹Department of Geological Sciences, University of Alabama; Tuscaloosa, AL USA

6 ²Upstream Tech, Natel Energy Inc.; Alameda, CA USA

7 ³LIT AI Lab & Institute for Machine Learning, Johannes Kepler University; Linz, Austria

8 ⁴Department of Geography, University of Alabama; Tuscaloosa, AL USA

9 **Key Points:**

- 10 • Post-processing the NWM with deep learning improves mean daily predictions of
11 surface runoff
- 12 • The LSTM post-processor improves representation the catchment hydrologic sig-
13 nature from the NWM and LSTM
- 14 • Post processing improvements are predictable from NWM performance and hy-
15 drologic signatures

Corresponding author: Jonathan Frame, jmframe@crimson.ua.edu

Abstract

The U.S. National Water Model (NWM) is a large scale hydrology simulator. Although NWM achieves coupling of multi-scale hydrological processes, its predictability at individual catchments can be improved. Hydrologic post-processing is an approach to reduce systematic simulation errors with statistical models, and has been shown to improve forecast accuracy of both calibrated and uncalibrated models. In this experiment we trained a Long Short-Term Memory (LSTM) network to post-process the NWM output, and tested performance at 531 basins across the continental United States. The LSTM post-processor provided a significant benefit to nearly all aspects of NWM streamflow predictions. The LSTM also benefited from NWM input - in particular, representation of hydrologic signatures improved, which indicates better representation of physical flow patterns.

1 Introduction

The U.S. National Water Model (NWM), based on WRF-Hydro (Cosgrove et al., 2015), is an emerging large scale hydrology simulator with 2.7 million river reaches. Some specific details of the NWM advancements in large scale hydrology are described by Elmer (2019, page 11), including increased resolution and number of stream reaches for a model covering this spatial domain. A strength of WRF-Hydro is simulating hydrologic dynamics (timing of the response) (Salas et al., 2018). The NWM is a useful tool in terms of hydrology over large spatial domains, but the performance has been shown to vary widely (Hansen, Shafiei Shiva, McDonald, & Nabors, 2019). Hansen et al. (2019) evaluated the performance of the NWM in the Colorado River Basin in terms of drought and low flows; they found better performance in the upper basin than the lower basin, and attributed the discrepancy to the NWM's success simulating snowpack hydrology. WRF-Hydro's performance at a regional scale show poor performance in the Southwest and Northern Plains (Salas et al., 2018). Sources of error in WRF-hydro may come from lakes, reservoirs, floodplain dynamics and soil parameter calibration (Salas et al., 2018).

The NWM version 2.0 is calibrated at 1,457 basins within the large scale domain of the Continental United States (CONUS). The USGS records daily streamflow at 28,529 sites¹. Calibrating the model at each stream gauge within CONUS would be a prohibitively large computational expense. Regionalizing calibrated basins can be used to improve forecast accuracy without having to calibrate each individual basin, but the accuracy in problematic regions would suffer (*e.g.*, Lower Colorado River and the Southwest). In the current stage of the NWM development the community should seek efficient and robust techniques to 1) make the best forecasts possible, and 2) maintain an agility and adaptability to future research which may continually increase forecast quality. There are promising results in the data science realm that may be directly (and immediately) applicable to the NWM.

Machine learning (ML) is gaining popularity in hydrological science, and there has been a call to merge ML with traditional hydrological modeling Reichstein et al. (2019). The Long Short-Term Memory network (LSTM) (Hochreiter, 1991; Hochreiter & Schmidhuber, 1997) is a time series deep learning method that is particularly well suited to model hydrologic processes (Kratzert, Klotz, Brenner, Schulz, & Herrnegger, 2018). LSTMs have been effective at simulating predictions of surface runoff at the daily time scale (Kratzert, Klotz, Shalev, et al., 2019), including in ungauged catchments where traditional methods of calibration do not work (Kratzert, Klotz, Herrnegger, et al., 2019). One potential problem with ML, however, is that it lacks a physical basis. While there are emerging efforts in hydrology to merge physical understanding with machine learning (*e.g.*, Chadalawada, Herath, & Babovic, 2020; Daw et al., 2020; Pelissier, Frame, & Nearing, 2020; Tartakovsky,

¹ <https://nwis.waterdata.usgs.gov/nwis>

64 Marrero, Perdikaris, Tartakovsky, & Barajas-Solano, 2020), *theory informed machine learning*
 65 (Karpatne et al., 2017) is still relatively immature in hydrology.

66 Hydrologic post-processing is a straightforward theory-informed machine learning
 67 approach which avoids the problems of calibration across large spatial domains. This ap-
 68 proach can remove systematic errors in the model prediction, and has been shown to im-
 69 prove forecast accuracy of both calibrated and uncalibrated basins, particularly in wet
 70 basins (Ye, Duan, Yuan, Wood, & Schaake, 2014). The general methodology of post-processing
 71 involves taking the output of a process-based model and feeding it into a data-driven model.
 72 We suggest an immediate step for improving NWM forecast accuracy without the compu-
 73 tational expense of calibration is post-processing streamflow predictions with ML. In
 74 this paper we apply a LSTM-based post processor for the NWM to improve basin-scale
 75 streamflow predictions.

76 The LSTM post-processor was applied to 531 basins across the CONUS. The basins
 77 chosen for this large scale analysis are mostly without engineered control structures, such
 78 as dams, canals, and levees. This was a deliberate choice made for the purpose of sim-
 79 ulating a close-to-natural rainfall-runoff response. Our goal is to learn about basin-scale
 80 rainfall-runoff processes, rather than the hydraulic engineering implications resulting from
 81 simulated controlled flow, *e.g.* a reservoir release. Kim et al. (2020) show the limitation
 82 of the NWM to predict streamflow in a highly engineered watershed and the need for
 83 representing controlled releases. Thus we are using some of the simplest, and top per-
 84 forming, applications of the NWM for these experiments.

85 2 Methods

86 2.1 Data and models

87 2.1.1 Camels catchments

88 This study uses the Catchment Attributes and Meteorological dataset for Large
 89 Sample Studies (CAMELS) (CAMELS; Addor, Newman, Mizukami, & Clark, 2017; New-
 90 man et al., 2015). These data have been curated by the US National Center for Atmo-
 91 spheric Research (NCAR) ². We used 531 of the 671 basins - these were the same basins
 92 used by Newman et al. (2015), who excluded basins with large discrepancies in differ-
 93 ent methods for measuring basin area and also basins larger than 2,000 km^2 . CAMELS
 94 data include corresponding daily streamflow records from United States Geological Sur-
 95 vey (USGS) gauges, and meteorological forcing data (precipitation, max/min temper-
 96 ature, vapor pressure and total solar radiation) come from North American Land Data
 97 Assimilation System (NLDAS; Xia et al., 2012).

98 2.1.2 National Water Model

99 We used the National Water Model version 2.0 reanalysis, which contains output
 100 from a 25-year retrospective simulation (January 1993 through December 2019)³. The
 101 NWM retrospective ingests rainfall and ingested other meteorological forcings from at-
 102 mospheric reanalyses⁴. NWM output includes streamflow (point fluxes) and land sur-
 103 face (gridded) states and fluxes. The specific features that we used from the NWM out-
 104 put are shown in Table 1. To be compatible with the LSTM model, which uses a one-
 105 day timestep, we took the mean values across the calendar day (12AM - 11PM) to pro-
 106 duce daily records from the hourly NWM output. Channel routing point data (CHRT)
 107 was collected at the NWM stream reach that corresponds to the stream gauge associ-

² <https://ral.ucar.edu/solutions/products/camels>

³ <https://docs.opendata.aws/nwm-archive/readme.html>

⁴ <https://water.noaa.gov/about/nwm>

108 ated with each CAMELS catchment. Gridded land surface data (LDAS) was collected
 109 from each 1 km^2 Noah-MP cell contained within the boundaries of each CAMELS catch-
 110 ment, and these were averaged to produce a single representative (lumped) value for each
 111 catchment. Gridded routing data were similarly collected from each 250 m^2 cell, and we
 112 also included the maximum value within the catchment boundary. We did not include
 113 lake input and output fluxes because these would be inconsistent across basins (some basins
 114 have zero and some basins have multiple lakes). Note that the units of the NWM out-
 115 puts are not required for the LSTM post-processor.

Table 1. National Water Model Output Data

Feature name	Feature	Resolution
ACCET	Accumulated evapotranspiration	1Km
FIRA	Total net long wave (LW) radiation to atmosphere	1Km
FSA	Total absorbed Short Wave (SW) radiation	1Km
FSNO	Snow cover fraction on the ground	1Km
HFX	Total sensible heat to the atmosphere	1Km
LH	Latent heat to the atmosphere	1Km
SNEQV	Snow water equivalent	1Km
SNOWH	Snow depth	1Km
SOIL M	Volumetric soil moisture	1Km
SOIL W	Liquid volumetric soil moisture	1Km
TRAD	Surface radiative temperature	1Km
UGDRNOFF	Accumulated underground runoff	1Km
streamflow	River Flow	point
q_lateral	Runoff into channel reach	point
velocity	River Velocity	point
qSfcLatRunoff	Runoff from terrain routing	point
qBucket	Flux from ground water bucket	point
qBtmVertRunoff	Runoff from bottom of soil to ground water bucket	point
sfheadsbrt	Ponded water depth	250Km
zwatablbrt	Water table depth	250Km

116

117 2.2 Long Short-Term Memory network

118 The LSTM takes two types of inputs: daily meteorological forcings and static catch-
 119 ment attributes. Again, note that the units of the forcing data are irrelevant when used
 120 as inputs for the LSTM, which does not include a mass or energy balance. We used eigh-
 121 teen catchment attributes from the CAMELS dataset related to climate, vegetation, to-
 122 pography, geology, and soils. These are described in more detail by Addor et al. (2017)
 123 and listed in Table 2. Catchment attributes are static for each basin (do not change in
 124 time). We trained the LSTM with the the features described in Table 1 of Kratzert, Klotz,
 125 Herrnegger, et al. (2019). For a detailed explanation of the LSTM itself see (Kratzert
 126 et al., 2018).

127 For the post-processing runs we added the states, fluxes, and streamflow predic-
 128 tions from version 2.0 of the NWM. We trained the LSTM on water years 2004 through
 129 2014 and tested the predictions on out-of-sample water years 1994 through 2002. The
 130 LSTM uses a 365-day LSTM look-back period, so a full year gap was left between train-
 131 ing and testing to prevent bleedover (*i.e.* information exchange) between the two peri-
 132 ods. We trained separate LSTMs with ten unique random seeds for initializing weights
 133 and biases, and calculated benchmarking statistics using the ensemble mean hydrograph.

134 The LSTM makes predictions representing streamflow in units mm , reflecting an area
 135 normalized volume of water that moves through a stream at each model timestep. USGS
 136 gauge records (and the NWM predictions) are in units m^3/s . We used the geospatial fab-
 137 ric estimate of catchment area provided in the CAMELS dataset to convert all stream-
 138 flow to units mm for our diagnostic comparison.

139 2.3 Experimental design

140 A simple schematic of the LSTM used as a post-processor for the NWM stream-
 141 flow prediction is shown in Figure 1. The LSTM post-processor takes the NWM outputs
 142 as inputs, and the result is a LSTM-based streamflow prediction that is influenced by
 143 the process-based NWM.

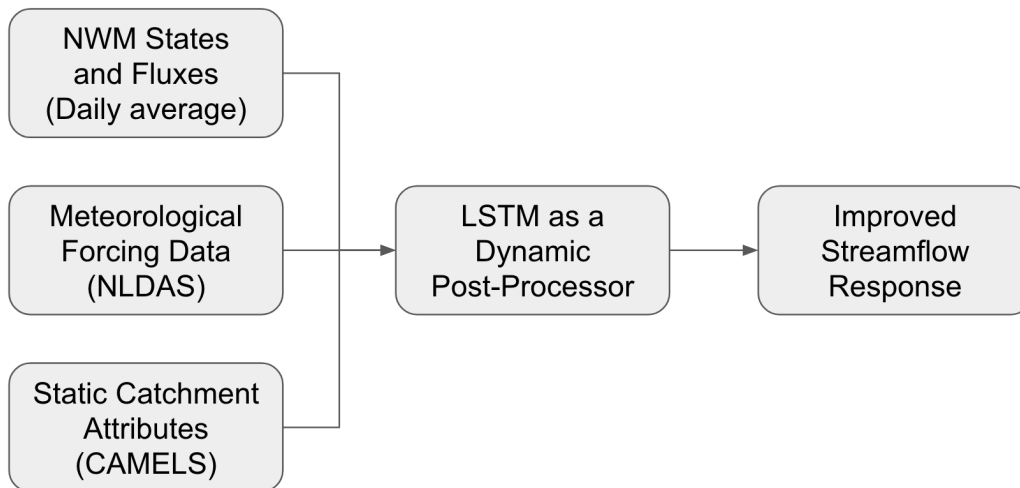


Figure 1. Flow chart showing the LSTM used as a post-processor for the NWM streamflow prediction.

144 As a quality check, we compared the results from each LSTM ensemble member,
 145 and found a relative standard error of the mean streamflow about 1%, and relative stan-
 146 dard error of the NSE value of about 0.01%. This means that all LSTM solutions are
 147 similar between random initialization seeds. Gauch, Mai, and Lin (2019) attributed a
 148 0.01 discrepancy in NSE values of the LSTM predictions to non-determinism of the loss
 149 function minimization. What Gauch et al. (2019) described as non-determinism exists
 150 as a result of the random seed, but running the training procedure twice with the same
 151 random seed gives an identical solution, satisfying the definition of determinism.

152 2.3.1 Performance metrics

153 We calculated a number of metrics for a robust evaluation of the predictive per-
 154 formance, including the NSE and KGE values (Ritter & Muñoz-Carpena, 2013). The vari-
 155 ance, bias and Pearson correlation metrics were calculated separately as components of
 156 the NSE Gupta, Kling, Yilmaz, and Martinez (2009); these tell us about relative vari-
 157 ability, mass conservation and linear correlation between the modeled/observed stream-
 158 flow values, respectively. The metrics were calculated in two ways: 1) at each basin and
 159 then averaged together, and 2) using all of the flows from all basins combined.

160 Our graphical results focus on three performance metrics: (i) Nash–Sutcliffe Ef-
 161 ficiency measures the overall predictive performance as a correlation coefficient for the

Table 2. Table of LSTM Inputs

Meteorological Forcing Data	
Maximum Air Temp	2-meter daily maximum air temperature [$^{\circ}C$]
Minimum Air Temp	2-meter daily minimum air temperature [$^{\circ}C$]
Precipitation	Average daily precipitation [mm/day]
Radiation	Surface-incident solar radiation [W/m^2]
Vapor Pressure	Near-surface daily average [P_a]
Static Catchment Attributes	
Precipitation Mean	Mean daily precipitation.
PET Mean	Mean daily potential evapotranspiration
Aridity Index	Ratio of Mean PET to Mean Precipitation Estimated by representing annual precipitation and temperature as sin waves Positive (negative) values indicate precipitation peaks during the summer (winter). Values of approx. 0 indicate uniform precipitation throughout the year.
Snow Fraction	Fraction of precipitation falling on days with temp $< 0^{\circ}C$.
High Precipitation Frequency	Frequency of days with $\leq 5 \times$ mean daily precipitation Average duration of high precipitation events (number of consecutive days with $\leq 5 \times$ mean daily precipitation).
Low Precip Frequency	Frequency of dry days (≤ 1 mm/day). Average duration of dry periods (number of consecutive days with precipitation ≤ 1 mm/day).
Elevation	Catchment mean elevation.
Slope	Catchment mean slope.
Area	Catchment area.
Forest Fraction	Fraction of catchment covered by forest.
LAI Max	Maximum monthly mean of leaf area index.
LAI Difference	Difference between the max. and min. mean of the leaf area index.
GVF Max	Maximum monthly mean of green vegetation fraction. Difference between the maximum and minimum monthly mean of the green vegetation fraction.
Soil Depth (Pelletier)	Depth to bedrock (maximum 50m).
Soil Depth (STATSGO)	Soil depth (maximum 1.5m).
Soil Porosity	Volumetric porosity.
Soil Conductivity	Saturated hydraulic conductivity.
Max Water Content	Maximum water content of the soil.
Sand Fraction	Fraction of sand in the soil.
Silt Fraction	Fraction of silt in the soil.
Clay Fraction	Fraction of clay in the soil.
Geological Permeability	Fraction of the catchment area characterized as “carbonate sedimentary rocks”. Surface permeability (log10).

162 1:1 linear fit between simulations and observations, (ii) Peak Timing Error measures the
 163 absolute value of differences (in units days) between simulated and observed peak flows
 164 for a given event, and (iii) Total Bias measures the overall bias of the simulated hydro-
 165 graph relative to observations and represents how well the model matches the total vol-
 166 ume of partitioned rainfall that passes through the stream gauge at each basin.

167 We also calculated performance metrics on different flow regimes. Rising limbs and
 168 falling limbs were characterized by a one-day derivative, where positive derivatives were
 169 categorized as rising limb, and negative derivatives as falling limb. High flows were char-
 170 acterized as all flow above the 80th percentile in a given basin, and low flows as below
 171 the 20th percentile in a given basin.

172 We tested the performance of the LSTM post-processor in different regions. We split
 173 the basins by USGS region⁵, and averaged the NSE, bias and timing error of the CAMELS
 174 basins within each region.

175 We set an alpha value for statistical significance to $\alpha = 0.05$. To control for mul-
 176 tiple comparisons we adjusted the alpha values using family-wise error rate equal to $1 -$
 177 $(1 - \alpha)^m$, with m being the number of significance tests (86), which brought our effec-
 178 tive alpha value down to 0.049. We tested for statistical significance with a Wilcoxon
 179 signed-rank test against the null hypothesis that our test model (LSTM post-processor)
 180 performance across basins came from the same distribution as our base models (NWM
 181 and LSTM).

182 ***2.3.2 Simulated hydrograph representation of hydrologic signatures***

183 Hydrologic signatures help us understand how well a model represents important
 184 aspects of real world streamflow, and where improvement should be made to the model's
 185 conceptualization Gupta, Wagener, and Liu (2008). We calculated the signatures listed
 186 in Table 2 of Addor et al. (2018) with model predicted values of streamflow. We calcu-
 187 lated the true hydrologic signatures from USGS streamflow observations. The compar-
 188 ison between true values and predicted values was made with the correlation coefficient
 189 (r^2), higher values indicating better representation of hydrologic signature across basins
 190 by the model. We used the Steiger method to test for statistically significance improve-
 191 ment (or detriment) between the base models and the LSTM post-processor (Steiger &
 192 Browne, 1984).

193 ***2.3.3 Identifying basins best suited for post-processing with Random For- 194 est regression***

195 The LSTM post-processor did not improve performance at every basin. It is there-
 196 fore valuable to know if the LSTM post-processor will work in any particular basin be-
 197 fore implementation. We trained a random forest regression to predict the performance
 198 change between the LSTM and the LSTM post-processor at each individual basin. The
 199 inputs to the regression analysis were the performance score of the NWM streamflow pre-
 200 dictions, hydrologic signatures and catchment characteristics. These regressors are use-
 201 ful to help interpret what basins might benefit most from the LSTM post-processor. We
 202 trained and tested random forests using k-fold cross-validation with 20 splits ($k = 20$)
 203 over the 531 basins. We report the correlation (r^2) of out-of-sample random forest pre-
 204 dictions of post-processing improvements vs. real post-processing improvements. We also
 205 calculated the mean decrease in impurity (or Gini importance) to determine the total
 206 reduction of the criterion brought by each feature.

⁵ <https://water.usgs.gov/GIS/regions.html>

207 **2.3.4 Interpretation of LSTM with integrated gradients**

208 We calculated integrated gradients (Sundararajan, Taly, & Yan, 2017) to attribute
 209 the LSTM inputs (both atmospheric forcings and NWM outputs) to the total predic-
 210 tion of streamflow. Integrate gradients are a type of sensitivity analysis that are rela-
 211 tively insensitive to low gradients (e.g., at the extremes of neural network activation func-
 212 tions). Integrated gradients are calculated separately for each input, at each timestep,
 213 for each lookback timestep, in each basin. This means that for 9 years of test data with
 214 a 365-day lookback there are about 1.2 million integrated gradients per input, per basin.

215 **2.3.5 Interpretation of LSTM with correlations between performance**
 216 **and NWM inputs**

217 We made a direct connection between LSTM post-processor improvements with
 218 the NWM outputs using correlation. We calculated Pearson R values between the basin
 219 average value of each NWM input feature and the total performance change (NSE, bias
 220 and peak timing). These correlations were calculated for different flow regimes (all flows,
 221 rising/falling limbs, and high/low flows. The strengths of these correlations (positive or
 222 negative) indicate which types of basins (via NWM features) are benefiting most from
 223 the LSTM post-processor.

224 **3 Results**

225 **3.1 Predictive performance**

226 Post-processing the NWM with LSTMs significantly improved predictive perfor-
 227 mance. Figure 2 shows the cumulative distributions of three performance metrics (Nash–Sutcliffe
 228 Efficiency, Peak Timing Error, and Total Bias). Figure 2 also shows scatter plots com-
 229 paring the performance of different models and includes r^2 values.

230 The LSTM post-processor improved the NSE score of the NWM mean daily stream-
 231 flow at a total of 495 (93%) and reduces accuracy in 36 basins (7%) of the total 531 CAMELS
 232 basins. The LSTM post-processor improved the total bias of the NWM mean daily stream-
 233 flow at a total of 331 (62%) of basins and the NWM mean daily streamflow at a total
 234 of 498 (94%) of basins. Improvements to performance in each basin are plotted spatially
 235 in Figure 3.

236 The LSTM post-processor improved predictions from the standalone LSTM in about
 237 half of the basins. The NSE score increased in a total of 299 (56%) and decreased in 232
 238 basins (44%) of the 531 basins. Total bias improved in 258 (49%) of the basins. Peak
 239 timing improved in 234 (44%) and was a detriment in 222 (42%) of the basins. Perfor-
 240 mance improvements relative to the standalone LSTM are plotted spatially in Figure 4.

241 **3.2 Performance by flow regime**

242 The LSTM post-processor improved predictive performance of the NWM accord-
 243 ing to the NSE and KGE metrics, as well as their components (variance and correlation).
 244 A full set of performance metrics broken down by flow regime are shown in 4. The left
 245 side of the table shows the average of metrics calculated individually at each basin, and
 246 right side of the table shows the metrics as calculated combining the flows from all basins.
 247 The Nash-Suttcliffe Efficiency includes both mean and median averages, but the rest of
 248 the metrics are only averaged by median. Failure to reject the null hypothesis of signif-
 249 icance (that the test model, LSTM post-processor, is different than the base models, NWM
 250 LSTM) is denoted by an asterisk.

251 In general this table shows that the performance of the LSTM post-processor is an
 252 improvement over the NWM in nearly all flow regimes, and by most metrics. The LSTM

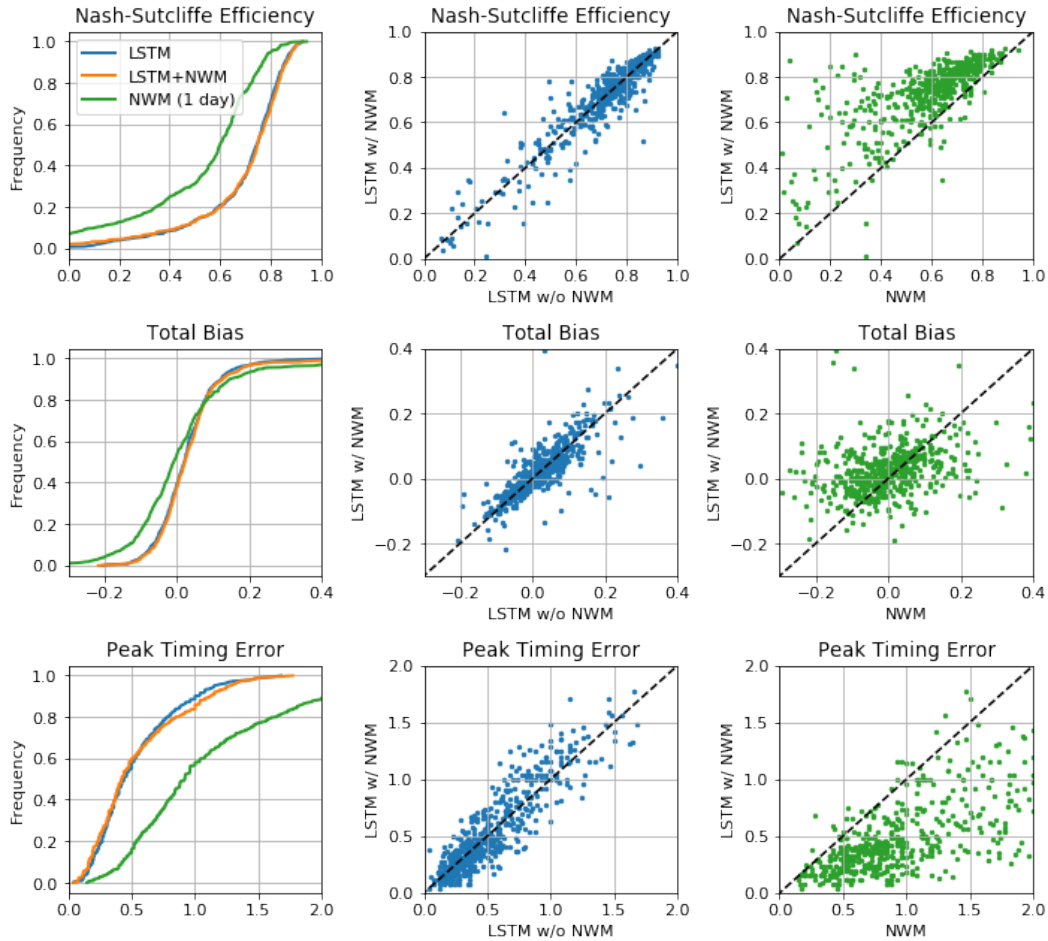


Figure 2. Results showing the cumulative distributions of model performance (Nash-Sutcliffe Efficiency, Total Bias and Peak Timing Error) over a 10-year test period in 531 CAMELS catchments. NWM is the National Water Model reanalysis averaged daily, LSTMs are Long Short Term Memory networks, and the LSTM w/ NWM represents the machine learning post-processed model with NWM inputs.

253 post-processor also improves upon the LSTM at a majority of the basins, and by most
 254 metrics. The rising limb and high flow regimes were improved by the LSTM post-processor
 255 according to every metric.

256 Bias is the only metric that was reduced due to post-processing, and the difference
 257 was highest in low flow regimes. Flows below the 20th percentile are poorly predicted
 258 by all models. This is likely due to the fact that all models tend to have a difficulty pre-
 259 dicting zero streamflow, and the 101 basins with periods of zero streamflow are weigh-
 260 ing down the average. This will be discussed further in section 3.6 in terms of hydrologic
 261 signatures.

262 The right side of the table has better performance values than average of metrics
 263 calculated individually at each basin. This is a result of some of the better performing
 264 basins compensating for poorer performing basins, or from a different perspective, some
 265 basins have relatively poor performance which weighs down the average.

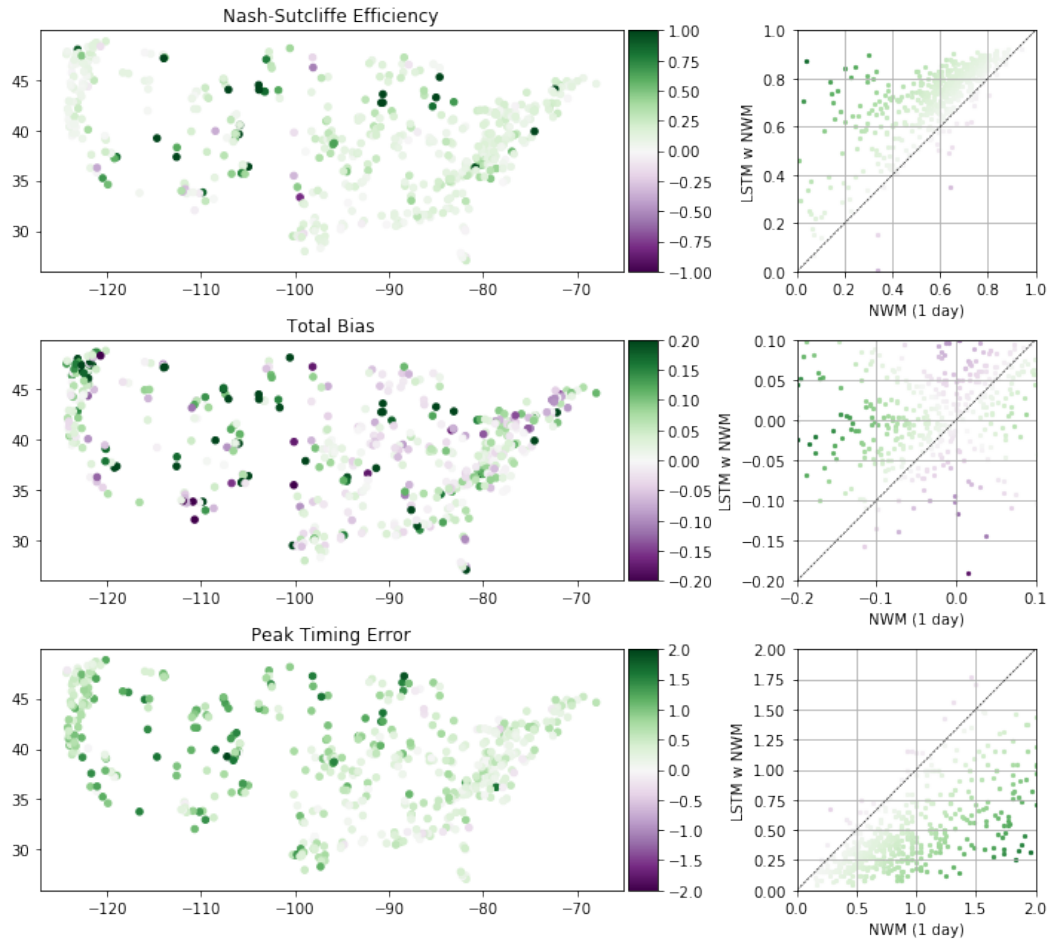


Figure 3. Improvements due to post-processing vs. the NWM in 531 CAMELS basins across CONUS. Green indicates basins where post-processing improved performance over the NWM (darker indicates larger relative improvement), and purple indicates basins where there was a decrease in performance (darker indicating worse relative detriment).

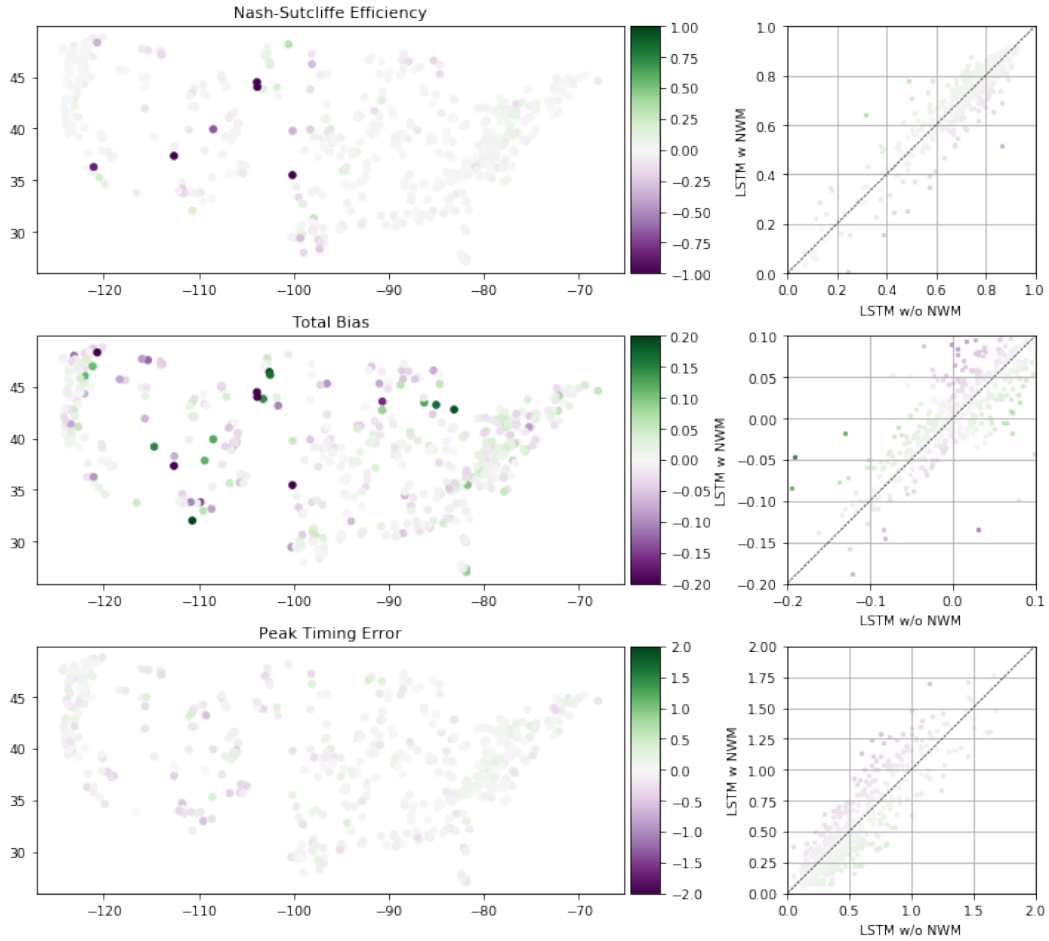


Figure 4. Improvements due to adding NWM states and fluxes as inputs into an LSTM in 531 CAMELS basins across CONUS. Green indicates basins where post-processing improved performance over the LSTM without NWM inputs (darker indicates larger relative improvement), and purple indicates basins where there was a decrease in performance (darker indicating worse relative detriment).

Table 3. Predictive performance for NWM, LSTM alone and the LSTM Post-processed NWM during various flow regimes.

Flow categories	Calculated Per-Basin						All Basins				
	NSE (mean)	NSE (median)	KGE	Variance	Bias	Pearson r	NSE	Variance	Bias	Pearson r	
All flows											
NWM	0.44	0.60	0.64	0.83	-0.01	0.80	0.74	0.85	-0.02	0.86	
LSTM	0.69	0.74	0.74	0.83	0.02	0.88	0.82	0.89	0.01	0.90	
LSTM+NWM	0.67**	0.75	0.76	0.87	0.02	0.88**	0.82	0.93	0.02	0.91	
Rising limbs											
NWM	0.46	0.58	0.55	0.73	-0.09	0.80	0.71	0.78	-0.07	0.85	
LSTM	0.66	0.71	0.72	0.80	-0.01	0.86	0.78	0.85	-0.01	0.88	
LSTM+NWM	0.65	0.72	0.74	0.85	0.00	0.87	0.79	0.89	-0.00	0.89	
Falling limbs											
NWM	0.23	0.57	0.64	1.03	0.06	0.83	0.77	0.97	0.02	0.88	
LSTM	0.69	0.78	0.77	0.92	0.05	0.90	0.87	0.96	0.03	0.93	
LSTM+NWM	0.65**	0.77**	0.77**	0.94	0.05	0.90**	0.87	0.98	0.03	0.93	
Above 80th percentile											
NWM	0.12	0.37	0.53	0.82	-0.12	0.70	0.67	0.83	-0.10	0.83	
LSTM	0.53	0.58	0.67	0.81	-0.08	0.81	0.78	0.86	-0.06	0.88	
LSTM+NWM	0.50**	0.60	0.69*	0.84	-0.07	0.81	0.79	0.90	-0.04	0.89	
Below 20th percentile											
NWM	-18424.98	-16.64	-1.88	3.68	1.88	0.37	0.39	1.30	0.22	0.82	
LSTM	-4749.68	-16.35	-1.31	2.85	3.27	0.43	0.56	1.26	0.33	0.89	
LSTM+NWM	-5147.62	-14.66	-1.24	2.85*	2.87	0.43	0.58	1.28	0.30	0.90	
	Post-Processing Helps the NWM										
	Post-Processing Hurts the NWM										
	NWM Hurts the LSTM										

* NWM post-processor is not significantly distinct from the NWM
 ** NWM post-processor is not significantly distinct from the LSTM

267

3.3 Performance by region

268

269

270

271

272

273

The LSTM post-processor significantly improves the NSE in fifteen of the eighteen regions. Note that region 9 is represented by only two CAMELS basins, which is not satisfactory for statistical evaluation. The bias was better represented by the NWM than the post-processor in five of the eighteen basins, including the entire East Coast (regions 1, 2 3), the Pacific Northwest (17) and the Lower-Colorado River (15). The timing was significantly improved at all regions with enough basins for a statistical evaluation.

Table 4. Predictive performance for NWM, LSTM alone and the LSTM Post-processed NWM in different regions.

Region	n	NSE		Bias		Timing		
		NWM	LSTM + NWM	NWM	LSTM + NWM	NWM	LSTM + NWM	
1	22	0.60	0.78	-0.05	0.07	0.66	0.32	
2	69	0.47	0.74	0.03	0.03	0.62	0.29	
3	79	0.54	0.71	0.02	-0.02	0.78	0.49	
4	30	0.42	0.69	0.00	0.05	1.13	0.64	
5	35	0.61	0.74	-0.04	0.03	0.63	0.35	
6	16	0.67	0.80	-0.01	0.00	0.73	0.24	
7	29	0.43	0.71	0.11	0.09	1.17	0.50	
8	7	0.61	0.67	0.01	-0.03	0.80	0.63	
9	2	0.29	0.40	-0.16	0.09	2.52	1.29	
10	49	-0.09	0.46	0.14	0.08	1.67	0.88	
11	22	0.29	0.56	0.05	0.04	1.07	0.60	
12	32	0.26	0.33	-0.01	-0.01	1.17	0.61	
13	7	0.24	0.63	0.16	0.09	2.14	1.17	
14	15	0.51	0.74	-0.03	0.01	2.12	1.01	
15	14	-0.03	0.33	-0.02	0.12	1.56	0.94	
16	5	0.22	0.71	-0.05	-0.03	1.82	0.89	
17	72	0.66	0.81	-0.03	0.04	1.14	0.46	
18	26	0.58	0.74	-0.03	0.00	1.35	0.58	
		Post-Processing significantly helps the NWM						
		Post-Processing significantly hurts the NWM						

274

275

3.4 Random Forest regression

276

277

278

279

280

281

282

We assessed the LSTM post-processor's potential for improving predictions over the NWM at each individual basins. Figure 5 shows the results predicting the post processor improvement at each basins with an r^2 value of 0.82 between the true values and the predicted values. The strength of this prediction is heavily weighted by the outlier basins with abnormally large performance improvements from the post-processor. This means that the LSTM post-processor can improve the predictions in the basins where the NWM does most poorly.

283

284

285

286

287

Figure 5 also shows the (Gini) importance of each regression. The r^2 value was the same with all hydrologic signatures included in the regression as it was with only the four top importance-ranked signatures (full analysis not shown). This figure shows the results when only those four signatures were used. The baseflow index is the signature with the highest importance for predicting if the LSTM post-processor will be beneficial.

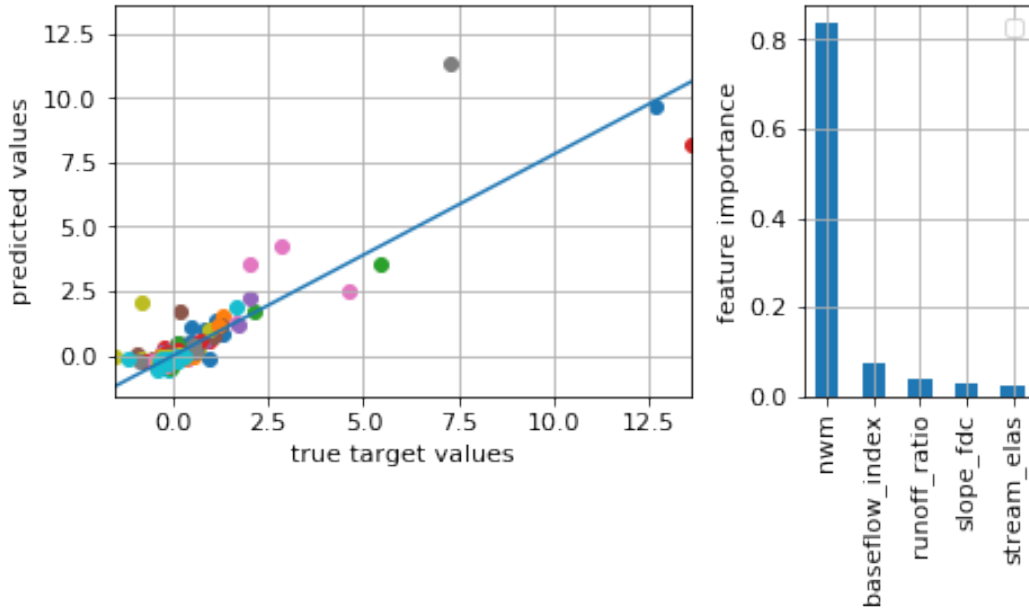


Figure 5. Predicting the LSTM post-processor improvement at each basin from with a random forest regression using NWM performance and hydrologic signatures as inputs. Left: Scatter plots for each of the 20 k-fold validation splits. Right: Average feature importance (across k-fold splits) on the prediction.

288 The aim of these results is understand whether it is possible to identify basins where
 289 post-processing might be beneficial. Although we found relatively high predictability in
 290 the improvement expected from post-processing, a problem is that we required know-
 291 ing ahead of time the NWM performance to do so. This prevents us from predicting post-
 292 processing improvement in *ungauged* basins, since calculating the NWM performance
 293 requires streamflow observations. Without the NWM performance as a predictor in this
 294 regression we achieve a r^2 value of 0.37 using all the hydrologic signatures and all the
 295 static catchment attributes together. (Figure 6). A total of 45 catchment attributes and
 296 signatures were included as regression inputs, but the figure shows only the Gini impor-
 297 tance of the top five. The baseflow index is again the most important signature for the
 298 regression, and the second signature being the slope of the flow duration curve. The basin
 299 area is the most important catchment characteristic, followed by the mean basin eleva-
 300 tion.

301 3.5 Integrated gradients

302 Figure 7 shows the relative strength of the total attribution of the dynamic inputs
 303 to the LSTM post processor averaged across the entire validation period and across each
 304 basin. The ordered magnitudes of the integrated gradients can be interpreted as corre-
 305 sponding to the order of importance of inputs. The most important dynamic features
 306 for the LSTM post-processor were: (i) precipitation from NLDAS, and (ii) routed stream-
 307 flow from the NWM point data. Precipitation inputs were weighted higher than the NWM
 308 streamflow output itself, which means that even when NWM streamflow data were avail-
 309 able, the LSTM learned to get information directly from forcings rather than from the
 310 NWM streamflow output. This indicates that the LSTM post-processor generates a new
 311 rainfall-runoff relationship rather than relying on the NWM, which makes some sense

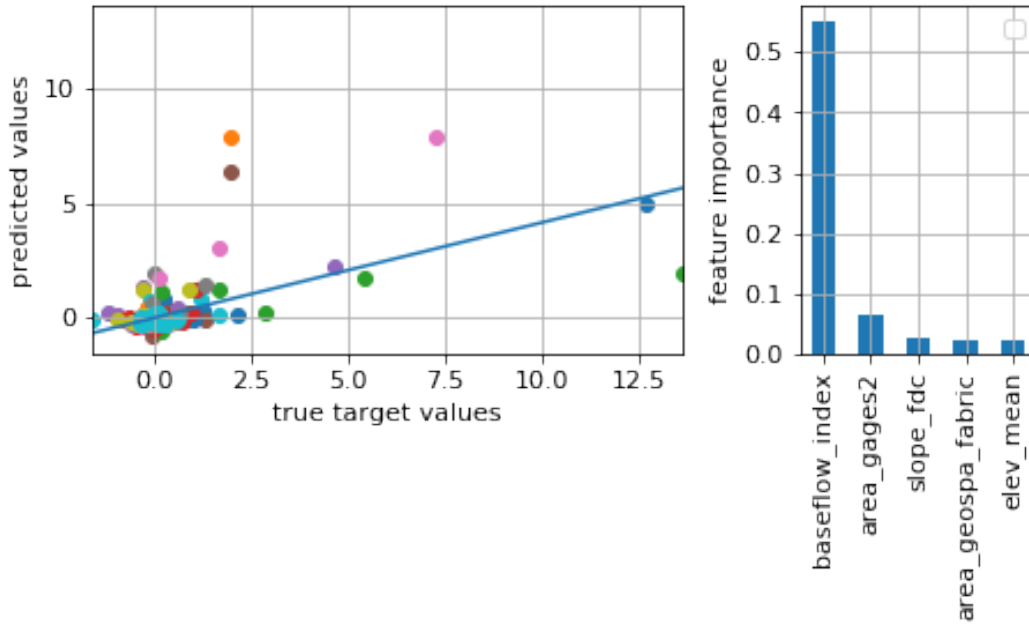


Figure 6. Predicting the LSTM post-processor improvement at each basin from with a random forest regression using static catchment attributes and hydrologic signatures as inputs. Left: Scatter plots for each of the 20 k-fold validation splits. Right: Top features ordered by Gini importance (averaged across k-fold splits) on the prediction.

312 given the overall results (Figure 2) that show similar performance between the LSTM
 313 with and without NWM inputs.

314 3.6 Correlations between NWM inputs and improvements

315 We need to show that the LSTM post-processor improves the predictions signif-
 316 icantly in all regions, to address our comment in the introduction about the regional cal-
 317 ibration being problematic in certain regions.

318 Figure 8 shows correlations (over 531 basins) between the time-averaged NWM in-
 319 puts and changes in NSE scores of the LSTM post-processor relative to both the LSTM
 320 alone and NWM alone. These correlations were calculated using the whole hydrograph.
 321 Results for rising limbs and falling limbs of the hydrograph were qualitatively similar to
 322 this figure, and were therefore omitted. The rows of this figure show that correlation was
 323 weaker for differences in NSE score than Total Bias and Peak Timing Error. Performance
 324 differences between the NWM and the LSTM post-processor were most strongly (anti)correlated
 325 with stream velocity and underground runoff: basins with lower stream velocity (veloc-
 326 ity) and less underground runoff (UGDRNOFF) saw greater performance improvement
 327 from (daily) post-processing. This means that in basins with high underground runoff
 328 and/or high stream velocity the LSTM post-processor improvements are smaller. In con-
 329 trast, basins with higher total radiation (TRAD) and higher latent heat flux (LH) saw
 330 greater improvement due to post-processing. This means that in basins with more ra-
 331 diation and heat flux the LSTM post-processor improvements are larger. A direct in-
 332 terpretation of this could be that a flat meandering stream in the Southwest will ben-
 333 efit from the LSTM post-processor, which is consistent with the findings of (Salas et al.,
 334 2018). Performance differences between the LSTM alone and the LSTM post-processor
 335 were most strongly correlated with snow water equivalent and snow depth. This is con-

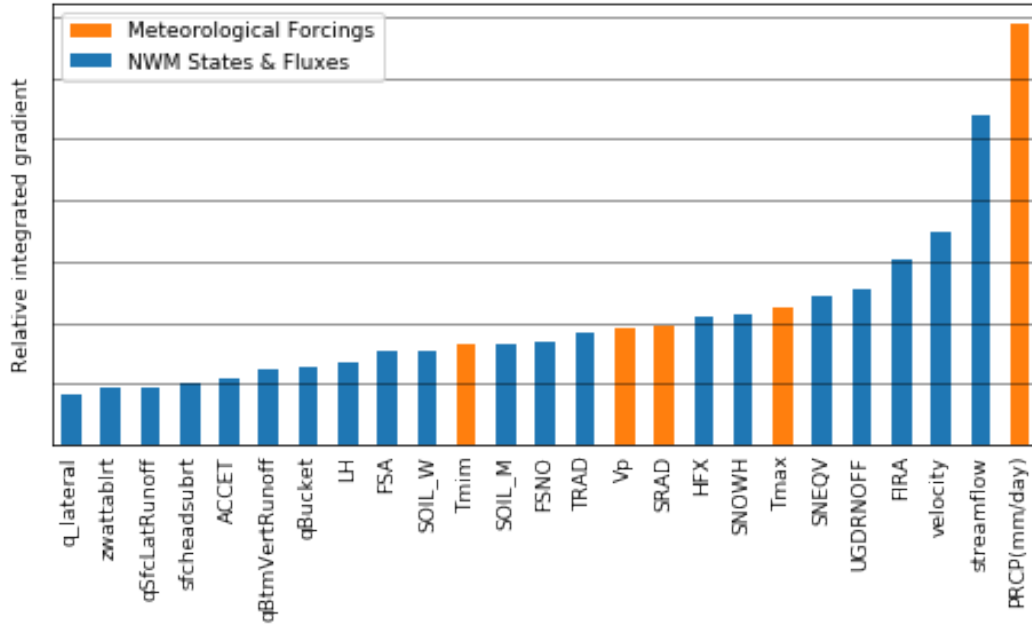


Figure 7. Attributions to the LSTM post-processor predictions. The vertical axis shows the relative magnitude of attribution (importance) for each input, with precipitation (PRCP) as the top contributor and NWM-predicted runoff into channel reach (q_{lateral}) contributing the least.

336 consistent with the findings of (Hansen et al., 2019) that the NWM represents snowpack hydrology well.
 337

338 3.7 Representations of hydrologic signatures

339 Results of the analysis of hydrologic signature representation are shown in Figure
 340 9, which also shows that the hydrologic signatures that at best represented by the NWM
 341 are similarly the best represented by the LSTM post-processor, and the same is true for
 342 the poorly represented hydrologic signatures. The overall r^2 values averaged across all
 343 signatures for the NWM, LSTM and LSTM post-processor were 0.59, 0.60 and 0.61, respec-
 344 tively.

345 The LSTM post-processor hurts the representation of the frequency of days with
 346 zero flow. There are 101 basins with any periods of zero flow. None of the models do well
 347 simulating zero flow, but the NWM is better at handling this situation, predicting zero
 348 flow periods at 56 basins. The LSTM and LSTM post-processor only predict periods of
 349 zero flows at 35 and 29 basins, respectively. This is an important characteristic in basins
 350 in the Southwest, where the NWM could use the benefit of the LSTM post-processor,
 351 so this would be a good place to focus future research of theory-guided ML for hydrology.
 352

353 The LSTM post-processor makes a significant improvement over the NWM for several
 354 signatures. The improvement of runoff ratio, which is the fraction of precipitation that
 355 makes it through the stream gauge at the surface, could be a compensation for the
 356 uncalibrated soil parameters mentioned by (Salas et al., 2018). The improvement of mean
 357 half-flow date. The LSTM post-processor improves both high and low flow representa-
 358 tions (5% 95% flow quantiles), which are important for natural resources management.
 359 The mean daily discharge is the best represented hydrologic signature by all models. This

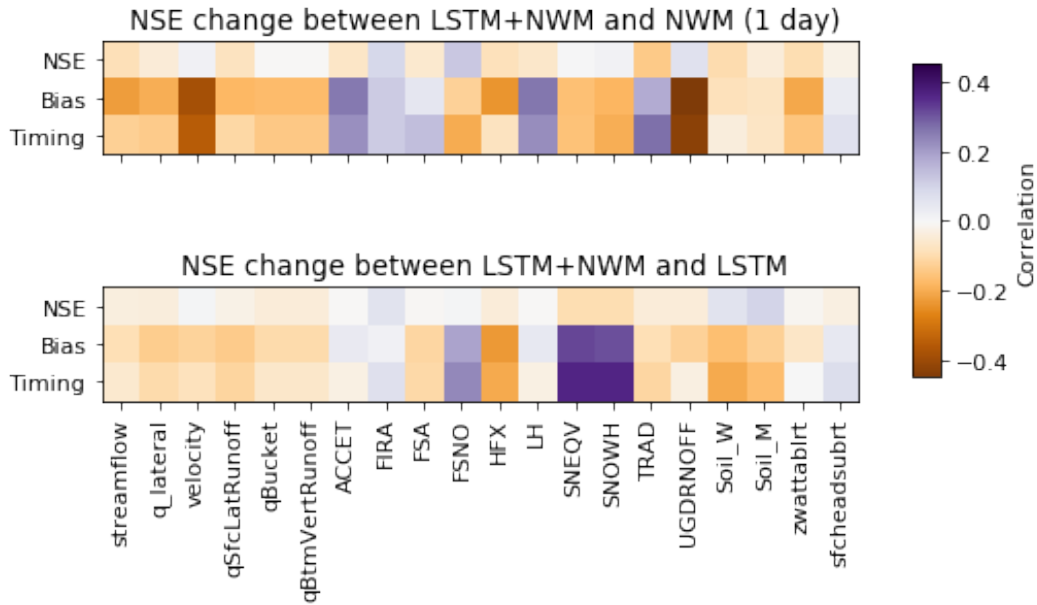


Figure 8. Correlations between the time-averaged NWM related inputs vs. NSE differences between the LSTM post-processor and both control models(LSTM alone and NWM alone).

360 is not surprising in terms of the LSTM and LSTM post-processor, because they were both
 361 trained to predict the mean daily discharge. It is also likely that the NWM calibrations,
 362 although not done at each basin, used mean daily discharge in the objective function.

363 The LSTM post-processor makes a significant improvement over the LSTM for base-
 364 flow index. This is the only signature which the LSTM post-processor improves both the
 365 NWM and the LSTM. This signature estimates the contribution of baseflow to the to-
 366 tal discharge, which is computed by hydrograph separation. (Klemeš, 1986) (summariz-
 367 ing Lindsly’s Applied Hydrology) cautions strongly against using hydrograph separation,
 368 because there is no real basis for distinguishing the source of flow in a stream. Even if
 369 the the baseflow index is only an coarse approximation of flow sources, the ability of the
 370 LSTM to improve on the representation, and even further by the LSTM post-processor,
 371 there is still some hydrologic conditions being represented.

372 4 Discussion

373 Results presented here show that the LSTM post-processor has potential to improve
 374 the daily averaged flow predictions of the NWM. The LSTM post-processor provided sig-
 375 nificant benefit to the NWM streamflow predictions at almost all (93%) of the 531 basins
 376 analyzed here. In the few basins where this was not the case, it may be possible to use
 377 fine tuning to calibrate a version of the post-processor that is specific to each gauge lo-
 378 cation (as would be done in traditional model calibration), however the LSTM post-processor
 379 used here can be applied to any basin, even ungauged. Right now, the post-processor
 380 is trained on naturalized basins, so further work would be needed to include reservoirs
 381 and other management practices. It is worth noting that the computational cost of train-
 382 ing the LSTM post-processor is many orders of magnitude lower than parameter esti-
 383 mation in a distributed model like the NWM, and the computational cost of forward pre-
 384 diction is negligible. Both training and prediction over all 531 basins used here can be
 385 done on a laptop in a few hours, if necessary (we used a small GPU cluster).

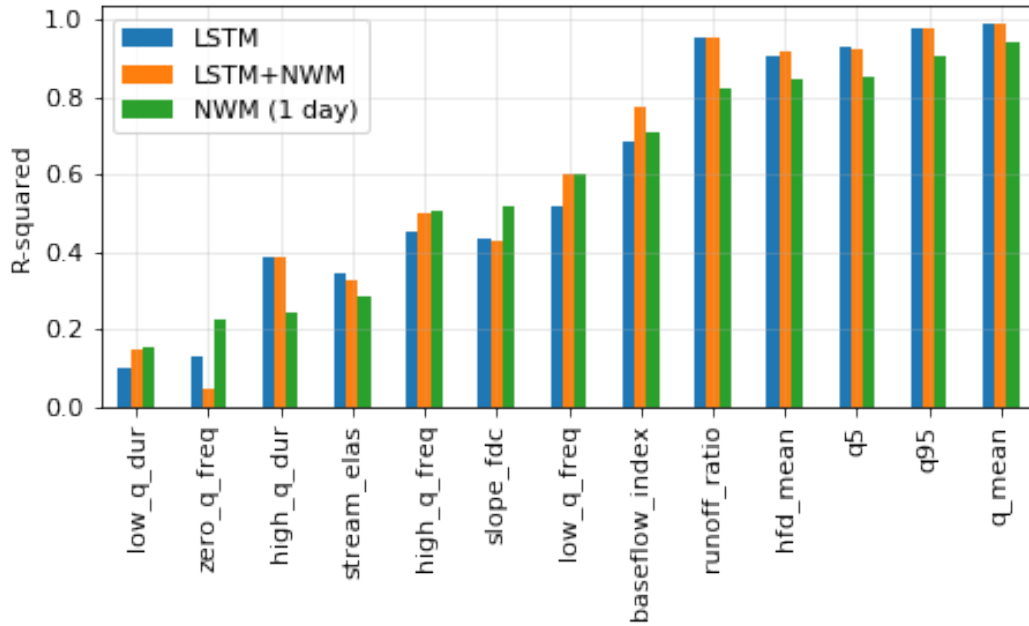


Figure 9. This plot shows the average representation of catchment hydrologic signatures by the NWM (blue), LSTM (orange) and the LSTM post-processor (green). The bars with the largest values represent the best performance.

386 The NWM performance and the performance improvement from the LSTM post-
 387 processor were negatively correlated: basins with low performance by the NWM have
 388 the highest performance change from the LSTM post-processor. This means that post-
 389 processing can be expected to correct situations where the NWM gives very bad predic-
 390 tions. Conversely, the performance of the NWM and the LSTM (without NWM)
 391 were not correlated. Considering also that the overall performance of the LSTM changed
 392 only minimally from the addition of the NWM inputs and that the LSTM still preferred
 393 to extract more information from precipitation forcings, we might conclude that the LSTM
 394 post-processor learned a new representation of the rainfall-runoff response. The overall
 395 improvement in the representation of hydrologic signatures indicates this new rainfall-
 396 runoff response is a better representation of physical flow patterns than either the NWM
 397 or the LSTM. The interpretation of the integrated gradient and the correlations between
 398 improvement and NWM features indicate that this improvement of flow patterns comes
 399 from information in the NWM representation of streamflow and snow states.

400 The NWM is not simply a rainfall-runoff simulator; it simulates flow through 2.7
 401 million river reaches around CONUS, dam operations, land surface processes, hydraulics,
 402 and other complications of large domain hydrology. The nature of the CAMELS catch-
 403 ments selected in these experiments are such that they have few man made control struc-
 404 tures, and are under 20,000 km^2 . The results presented in this paper show that the LSTM
 405 post-processor improved streamflow predictions in similarly undisturbed catchments. Kratzert,
 406 Klotz, Herrnegger, et al. (2019) show that these predictions extend into ungauged basins.
 407 The immediate potential for improving real-time forecasting could be deploying this post-
 408 processor in undisturbed catchments, and undisturbed sub-catchments upstream of un-
 409 natural hydrologic conditions such as dams, agriculture lands and urban centers. An im-
 410 mediate next step would be to develop a post-processor that aggregates surface and sub-
 411 surface runoff, but allows for the NWM router to aggregate these fluxes into streamflow.

412 This would allow for retaining conceptual representations of lakes and reservoirs that al-
413 ready exist in the NWM.

414 The post-processing procedure presented here is one of the more crude techniques
415 currently available for combining process-based and data-driven models. Several other
416 methods of combining the benefits of machine learning (predictability) with the bene-
417 fits of physically realistic hydrologic theory (robustness) are in development. For exam-
418 ple, (Pelissier et al., 2020) use Gaussian Processes to predict error between modeled and
419 observed soil moisture, which allows ML to be used dynamically within a land surface
420 model to correct the soil moisture state at each timestep of a simulation. Another ex-
421 ample is using physical principals to constrain the loss function of an ML model during
422 training. Implementing post-processing is relatively straightforward compared to other
423 techniques such as adding physics into ML code, or using ML to dynamically updating
424 the state variables.

425 **Data Availability Statement:**

426 All data and code used in this paper are publicly available in the following locations:

- 427 • U.S. National Water Model: [https://docs.opendata.aws/nwm-archive/readme](https://docs.opendata.aws/nwm-archive/readme.html)
428 [.html](https://docs.opendata.aws/nwm-archive/readme.html)
- 429 • CAMELS data: <https://ral.ucar.edu/solutions/products/camels>
- 430 • Data processing code: [https://github.com/jmframe/nwm-reanalysis-model-data](https://github.com/jmframe/nwm-reanalysis-model-data-processing)
431 [-processing](https://github.com/jmframe/nwm-reanalysis-model-data-processing)
- 432 • LSTM code: https://github.com/kratzert/ealstm_regional_modeling
- 433 • Post-processing and analysis code: [https://github.com/jmframe/nwm-post-processing](https://github.com/jmframe/nwm-post-processing-with-lstm)
434 [-with-lstm](https://github.com/jmframe/nwm-post-processing-with-lstm)

435 **Acknowledgments**

436 Authors from the Johannes Kepler University were partially supported by a Google fac-
437 ulty research award. Jonathan Frame from the University of Alabama was partially sup-
438 ported by the NASA Terrestrial Hydrology Program. Grey Nearing from the University
439 of Alabama was partially supported by the NCAR COMET program on a cooperative
440 award with the National Water Center.

441 **References**

- 442 Addor, N., Nearing, G., Prieto, C., Newman, A. J., Le Vine, N., & Clark, M. P.
443 (2018). A Ranking of Hydrological Signatures Based on Their Predictability in
444 Space. *Water Resources Research*(i), 8792–8812. doi: 10.1029/2018WR022606
- 445 Addor, N., Newman, A. J., Mizukami, N., & Clark, M. P. (2017). The CAMELS
446 data set: catchment attributes and meteorology for large-sample studies. *Earth*
447 *Syst. Sci.*, 21, 5293–5313. Retrieved from [https://www.hydrol-earth-syst](https://www.hydrol-earth-syst-sci.net/21/5293/2017/hess-21-5293-2017.pdf)
448 [-sci.net/21/5293/2017/hess-21-5293-2017.pdf](https://www.hydrol-earth-syst-sci.net/21/5293/2017/hess-21-5293-2017.pdf) doi: 10.5194/hess-21-5293
449 -2017
- 450 Chadalawada, J., Herath, H. M., & Babovic, V. (2020). Hydrologically Informed
451 Machine Learning for Rainfall-Runoff Modeling: A Genetic Programming-
452 Based Toolkit for Automatic Model Induction. *Water Resources Research*,
453 56(4), 1–23. doi: 10.1029/2019WR026933
- 454 Cosgrove, B., Gochis, D., Clark, E. P., Cui, Z., Dugger, A. L., Fall, G. M., . . . oth-
455 ers (2015). Hydrologic modeling at the national water center: Operational
456 implementation of the wrf-hydro model to support national weather service
457 hydrology. In *Agu fall meeting abstracts*.
- 458 Daw, A., Thomas, R. Q., Carey, C. C., Read, J. S., Appling, A. P., & Karpatne, A.
459 (2020). Physics-guided architecture (pga) of neural networks for quantifying

- 460 uncertainty in lake temperature modeling. In *Proceedings of the 2020 siam*
 461 *international conference on data mining* (pp. 532–540).
- 462 Elmer, N. J. (2019). *Using Satellite Observations of River Height and Vegetation*
 463 *to Improve National Water Model Initialization and Streamflow Prediction*
 464 (Unpublished doctoral dissertation). The University of Alabama in Huntsville.
- 465 Gauch, M., Mai, J., & Lin, J. (2019). The Proper Care and Feeding of CAMELS:
 466 How Limited Training Data Affects Streamflow Prediction. , *2342*, 0–2. Re-
 467 trieved from <http://arxiv.org/abs/1911.07249>
- 468 Gupta, H. V., Kling, H., Yilmaz, K. K., & Martinez, G. F. (2009). Decomposi-
 469 tion of the mean squared error and NSE performance criteria: Implications
 470 for improving hydrological modelling. *Journal of Hydrology*, *377*(1-2), 80–91.
 471 Retrieved from <http://dx.doi.org/10.1016/j.jhydrol.2009.08.003> doi:
 472 10.1016/j.jhydrol.2009.08.003
- 473 Gupta, H. V., Wagener, T., & Liu, Y. (2008). Reconciling theory with observations:
 474 elements of a diagnostic approach to model evaluation. *Hydrological Processes*,
 475 *2274* (November 2008), 2267–2274. doi: 10.1002/hyp.6989
- 476 Hansen, C., Shafiei Shiva, J., McDonald, S., & Nabors, A. (2019). Assessing Retro-
 477 spective National Water Model Streamflow with Respect to Droughts and Low
 478 Flows in the Colorado River Basin. *Journal of the American Water Resources*
 479 *Association*, *55*(4), 964–975. doi: 10.1111/1752-1688.12784
- 480 Hochreiter, S. (1991). *Untersuchungen zu dynamischen neuronalen netzen* (Unpub-
 481 lished doctoral dissertation). Technische Universität München.
- 482 Hochreiter, S., & Schmidhuber, J. (1997). Long short-term memory. *Neural Com-*
 483 *putation*, *9*(8), 1735–1780. Retrieved from [https://doi.org/10.1162/neco](https://doi.org/10.1162/neco.1997.9.8.1735)
 484 [.1997.9.8.1735](https://doi.org/10.1162/neco.1997.9.8.1735) doi: 10.1162/neco.1997.9.8.1735
- 485 Karpatne, A., Atluri, G., Faghmous, J. H., Steinbach, M., Banerjee, A., Ganguly,
 486 A., . . . Kumar, V. (2017). Theory-guided data science: A new paradigm for
 487 scientific discovery from data. *IEEE Transactions on Knowledge and Data*
 488 *Engineering*, *29*(10), 2318–2331.
- 489 Kim, J., Read, L., Johnson, L. E., Gochis, D., Cifelli, R., & Han, H. (2020). An
 490 experiment on reservoir representation schemes to improve hydrologic predic-
 491 tion: coupling the National Water Model with the HEC-ResSim. *Hydrolog-*
 492 *ical Sciences Journal*, *0*(0), 1. Retrieved from [https://doi.org/10.1080/](https://doi.org/10.1080/02626667.2020.1757677)
 493 [02626667.2020.1757677](https://doi.org/10.1080/02626667.2020.1757677) doi: 10.1080/02626667.2020.1757677
- 494 Klemeš, V. (1986). Dilettantism in hydrology: Transition or destiny? *Water Re-*
 495 *sources Research*, *22*(9 S), 177S–188S. doi: 10.1029/WR022i09Sp0177S
- 496 Kratzert, F., Klotz, D., Brenner, C., Schulz, K., & Herrnegger, M. (2018). Rainfall-
 497 runoff modelling using long short-term memory (lstm) networks. *Hydrology*
 498 *and Earth System Sciences*, *22*(11), 6005–6022.
- 499 Kratzert, F., Klotz, D., Herrnegger, M., Sampson, A. K., Hochreiter, S., & Nearing,
 500 G. S. (2019). Towards Improved Predictions in Ungauged Basins: Exploiting
 501 the Power of Machine Learning. *Water Resources Research*, 2019WR026065.
 502 Retrieved from [https://onlinelibrary.wiley.com/doi/abs/10.1029/](https://onlinelibrary.wiley.com/doi/abs/10.1029/2019WR026065)
 503 [2019WR026065](https://onlinelibrary.wiley.com/doi/abs/10.1029/2019WR026065) doi: 10.1029/2019WR026065
- 504 Kratzert, F., Klotz, D., Shalev, G., Klambauer, G., Hochreiter, S., & Nearing, G.
 505 (2019). Towards learning universal, regional, and local hydrological behaviors
 506 via machine learning applied to large-sample datasets. *Hydrology and Earth*
 507 *System Sciences*, *23*(12), 5089–5110. doi: 10.5194/hess-23-5089-2019
- 508 Newman, A. J., Clark, M. P., Sampson, K., Wood, A., Hay, L. E., Bock, A., . . .
 509 Duan, Q. (2015). Development of a large-sample watershed-scale hydrom-
 510 eteorological data set for the contiguous USA: Data set characteristics and
 511 assessment of regional variability in hydrologic model performance. *Hydrology*
 512 *and Earth System Sciences*, *19*(1), 209–223. doi: 10.5194/hess-19-209-2015
- 513 Pelissier, C., Frame, J., & Nearing, G. (2020). Combining parametric land surface
 514 models with machine learning. *arXiv preprint arXiv:2002.06141*.

- 515 Reichstein, M., Camps-valls, G., Stevens, B., Jung, M., Denzler, J., & Carvalhais,
 516 N. (2019). Deep learning and process understanding for data-driven Earth
 517 system science. *Nature*, *566*, 195 – 204. Retrieved from [http://dx.doi.org/](http://dx.doi.org/10.1038/s41586-019-0912-1)
 518 [10.1038/s41586-019-0912-1](http://dx.doi.org/10.1038/s41586-019-0912-1) doi: 10.1038/s41586-019-0912-1
- 519 Ritter, A., & Muñoz-Carpena, R. (2013). Performance evaluation of hydrolog-
 520 ical models: Statistical significance for reducing subjectivity in goodness-
 521 of-fit assessments. *Journal of Hydrology*, *480*, 33–45. Retrieved from
 522 <http://dx.doi.org/10.1016/j.jhydrol.2012.12.004> doi: 10.1016/
 523 [j.jhydrol.2012.12.004](http://dx.doi.org/10.1016/j.jhydrol.2012.12.004)
- 524 Salas, F. R., Somos-Valenzuela, M. A., Dugger, A., Maidment, D. R., Gochis, D. J.,
 525 David, C. H., ... Noman, N. (2018). Towards real-time continental scale
 526 streamflow simulation in continuous and discrete space. *JAWRA Journal of*
 527 *the American Water Resources Association*, *54*(1), 7–27.
- 528 Steiger, J., & Browne, M. (1984). The comparison of interdependent correlations be-
 529 tween optimal linear composites. *Psychometrika*, *49*(1), 11–24. doi: 10.1017/
 530 [CBO9781107415324.004](http://dx.doi.org/10.1017/CBO9781107415324.004)
- 531 Sundararajan, M., Taly, A., & Yan, Q. (2017). Axiomatic attribution for deep net-
 532 works. *34th International Conference on Machine Learning, ICML 2017*, *7*,
 533 5109–5118.
- 534 Tartakovsky, A. M., Marrero, C. O., Perdikaris, P., Tartakovsky, G. D., & Barajas-
 535 Solano, D. (2020). Physics-Informed Deep Neural Networks for Learning
 536 Parameters and Constitutive Relationships in Subsurface Flow Problems.
 537 *Water Resources Research*, *56*(5), 1–16. doi: 10.1029/2019WR026731
- 538 Xia, Y., Mitchell, K., Ek, M., Sheffield, J., Cosgrove, B., Wood, E., ... others
 539 (2012). Continental-scale water and energy flux analysis and validation for
 540 the north american land data assimilation system project phase 2 (nldas-2):
 541 1. intercomparison and application of model products. *Journal of Geophysical*
 542 *Research: Atmospheres*, *117*(D3).
- 543 Ye, A., Duan, Q., Yuan, X., Wood, E. F., & Schaake, J. (2014). Hydrologic post-
 544 processing of MOPEX streamflow simulations. *JOURNAL OF HYDROLOGY*,
 545 *508*, 147–156. Retrieved from [http://dx.doi.org/10.1016/j.jhydrol.2013.](http://dx.doi.org/10.1016/j.jhydrol.2013.10.055)
 546 [10.055](http://dx.doi.org/10.1016/j.jhydrol.2013.10.055) doi: 10.1016/j.jhydrol.2013.10.055